

Long-term interaction between mid-ocean ridges and mantle plumes

J. M. Whittaker^{1*}, J. C. Afonso², S. Masterton^{3†}, R. D. Müller⁴, P. Wessel⁵, S. E. Williams⁴ and M. Seton⁴

Plate tectonic motions are commonly considered to be driven by slab pull at subduction zones and ridge push at mid-ocean ridges, with motion punctuated by plumes of hot material rising from the lower mantle^{1,2}. Within this model, the geometry and location of mid-ocean ridges are considered to be independent of lower-mantle dynamics, such as deeply sourced plumes that produce voluminous lava eruptions—termed large igneous provinces². Here we use a global plate model³ to reconstruct the locations of large igneous provinces relative to plumes and mid-ocean ridges at the time they formed. We find that large igneous provinces repeatedly formed at specific locations where mid-ocean ridges and plumes interact. We calculate how much mantle material was converted to oceanic lithosphere at the mid-ocean ridges and find that slowly migrating ridge systems that have been stabilized by upwelling plumes have extracted large volumes of material from the same part of the upper mantle over periods up to 180 million years. The geochemical signatures of mid-ocean ridge basalts and seismic tomographic data show that upper-mantle temperatures are elevated at significant distances from ridge–plume interactions, indicating a far-field, indirect influence of plume–ridge interactions on the upper-mantle structure. We conclude that strong feedbacks exist between the dynamics of slowly migrating ridges and deeply sourced plumes.

It has long been recognized that mid-ocean ridges (MORs) migrate⁴ relative to the deep underlying mantle^{4,5}. Present-day MOR migration rates are known to be intimately related to seafloor morphology^{6–8} and the physical state of the upper mantle^{9,10}, with present-day migration rates correlating with asymmetric seafloor spreading⁶, ridge-crest lava generation⁷, melting asymmetry⁹, depth and geochemical discontinuity¹⁰, and ridge morphology⁸, but the influence of ancient ridge migration rates remains unknown.

Plumes have long been associated with mid-ocean ridges¹¹ and ridge–plume interaction is known to cause deviation from expected MOR migration rates (assuming symmetric spreading without affecting overall surface motions), with slower MOR migration rates recorded at spreading systems experiencing ridge–plume interactions¹². Reconstructing relative and absolute plate motions³ for the past 140 Myr reveals that MOR systems have experienced a variety of contrasting behaviours—combinations of stationary to rapidly migrating MORs coupled with a wide range of seafloor spreading rates. Slowly migrating, fast-spreading MORs extract significant volumes of melt from the same source region, whereas

rapidly migrating MORs extract relatively smaller volumes of melt across a broader source region.

The effects of long-term variations in MOR migration and the resulting non-uniform sampling of the upper mantle have not previously been studied, although there is growing evidence supporting close linkages between slowly migrating MORs and plumes at the present-day, including MORB geochemistry and upper-mantle seismic tomography¹³, mantle convection simulations¹⁴ and laboratory models¹⁵. Ridge–plume interactions have also previously been implicated in causing slow MOR migration rates for up to 70 Myr (ref. 12), via a ridge jump mechanism, where ridge–plume interactions are sustained by successive jumps by the MOR towards the plume. An alternative mechanism to facilitate interaction between ridges and plumes is plume capture, where plumes bend and flow towards migrating ridges, possibly induced by ridge suction, from distances of up to ~1,400 km (ref. 16).

Large igneous provinces (LIPs) are typically considered to be the product of a plume-head eruption¹⁷. They form on both continental and oceanic crust, which allows us to use LIPs (ref. 2; Fig. 1 and Supplementary Table 1 and Supplementary Fig. 1) to assess the longevity of plume interactions with both MORs and continental rift divergent plate boundaries and to demonstrate that ridge–plume interactions can continue for up to 180 Myr and strongly influence ridge migration rates.

We restore LIPs to their absolute location at their time of formation (Fig. 1 and Supplementary Fig. 2) and locate the closest plume and plate boundary (Fig. 1 and Supplementary Tables 1–2). Clusters of ≥ 3 LIPs occur above the edges of the large low-shear velocity provinces (LLSVPs; ref. 18) around nine individual ridge–plume interactions (Fig. 1a and Supplementary Figs 3 and 4). The LIPs attributed to these nine plumes comprise ~60% of the total LIP area. The plumes involved are all thought to be deeply sourced^{19,20}, with the exception of Marion, which we suggest may be a more likely candidate for being deeply sourced than the neighbouring (~1,000 km away) Crozet plume. Further, ~90% of analysed LIPs formed within 1,400 km of both a deeply sourced plume (~93%) and a diverging plate boundary or extensional continental region (~96%), a result strongly supportive of their formation proximal to a ridge–plume interaction (Fig. 1a).

Each LIP cluster exhibits a significant range (30–130 Myr) in the LIP formation times (Supplementary Table 2), supporting episodic LIP formation at the same ridge–plume interactions. This result supports the idea that plume magma flux can vary significantly through time²¹.

¹Institute for Marine and Antarctic Studies, University of Tasmania, Hobart, Tasmania 7001, Australia. ²Macquarie University, Sydney, New South Wales 2109, Australia. ³Leeds University, Leeds LS2 9JT, UK. ⁴School of Geosciences, University of Sydney, Sydney, New South Wales 2006, Australia. ⁵School of Ocean and Earth Science and Technology, University of Hawaii, Honolulu, Hawaii 96822, USA. [†]Present address: Getech Plc, Kitson House, Elmete Hall, Elmete Lane, Leeds LS28 2LL, UK. *e-mail: jo.whittaker@utas.edu.au

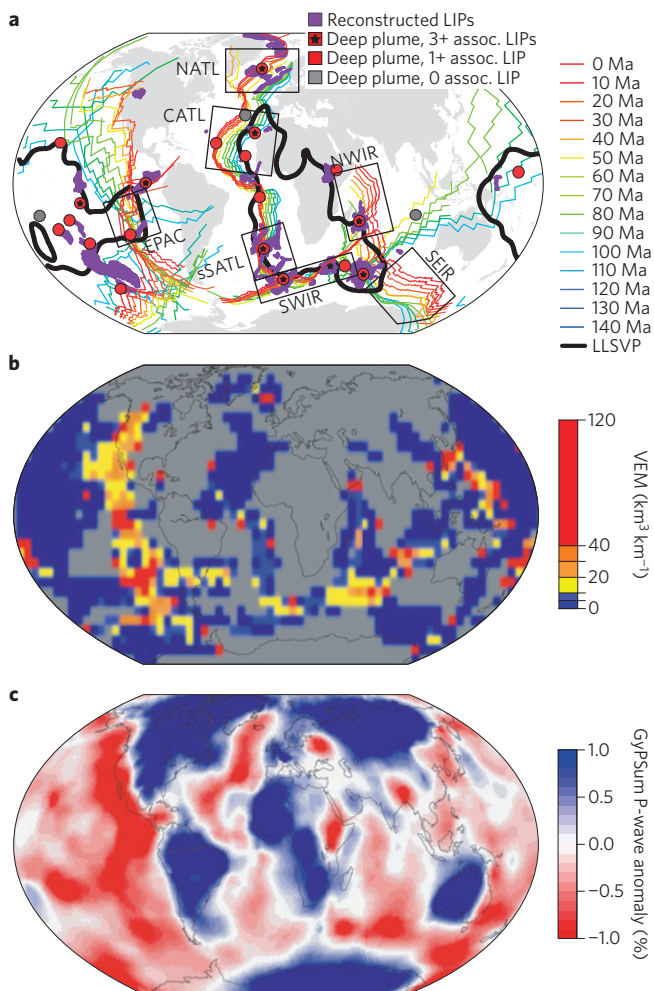


Figure 1 | Global data sets. **a**, Reconstructed absolute MOR locations (coloured lines), reconstructed LIPs (purple) cluster around hotspots (circles). LLSVP regions shown using the SMEAN tomography model 1% contour 92 km above the core-mantle boundary²⁸. Black boxes indicate where ridge migration was computed along flowlines. CATL—Central Atlantic, EPAC—East Pacific, NATL—North Atlantic, NWIR—Northwest Indian Ridge, SEIR—Southeast Indian Ridge, sSATL—southern South Atlantic, SWIR—Southwest Indian Ridge. **b**, Estimated upper-mantle VEM ($\text{km}^3 \text{km}^{-1}$ of overlying ridge). **c**, 100–175 km GypSum P-wave velocities²⁴.

Three of the ridge–plume interactions with clustered LIPs (Tristan da Cunha, Bouvet and Marion) are located along slowly migrating southern South Atlantic (sSATL) and Southwest Indian Ridge (SWIR) systems, and, in pre-Cenozoic times, the SWIR extended further east to include the Kerguelen plume, which also exhibits clustered LIPs. This pattern reveals that ridge–plume interactions in the sSATL and SWIR are remarkably stable, probably having existed since ~ 180 Myr ago (Ma), initially as interactions between plumes and divergent continental material, and surviving the transition from continental rifting to seafloor spreading. Our results support LIP formation above the edges of the African LLSVP (ref. 22), and suggest that in these locations diverging plate boundaries mirror the stable deep-Earth LLSVP geometries.

LIP clustering around ridge–plume interactions in the Pacific Ocean is less clear (Fig. 1a). A feasible explanation is that mantle upwelling at slower spreading ridges is strong enough to focus plumes towards the ridge but insufficiently strong to capture them entirely, enabling surface hotspots to form proximal to the MOR (ref. 15). In contrast, at fast-spreading ridges, plumes are more

commonly incorporated into the central upwelling, resulting in fewer distinct plumes proximal to the MOR (ref. 15), and possibly lower LIP formation.

We have developed and implemented a novel methodology (see Methods and Supplementary Figs 5–9) for constructing a global map of the relative volume of upper-mantle material extracted through partial melting at MORs since the Early Cretaceous period. We use this map to assess relationships of slowly migrating ridges caused by plume–ridge interactions with the thermal structure of the upper mantle.

Our map (Fig. 1b) is a proxy for the volume of extracted mantle (VEM) and is calculated as a function of the residence time (the duration for which a MOR lies above an area of upper mantle) of the global MOR system²³ and the rate at which material is extracted from the mantle (that is, the spreading rate).

Regions exhibiting high VEM values are indicative of prolonged melt extraction and mantle focusing/processing by a slowly migrating MOR system with moderate to fast spreading rates—for example, the Eastern Pacific. In contrast, rapid MOR migration, even with rapid spreading rates, does not result in high VEM values—for example, Wharton Basin, Central Atlantic, and Cenozoic Southeast Indian Ridge.

We observe particularly slow MOR migration rates over the past 100 Myr at three ridges that at present exhibit ridge–plume interactions, namely the East Pacific Rise (EPAC; Galapagos and Easter plumes), the SWIR (Marion/Crozet and Bouvet plumes), and the sSATL (Tristan da Cunha and Bouvet plumes). On average, these three MOR systems have migrated <500 km in an absolute sense since 100 Ma, compared with absolute migration distances of $>1,500$ – $2,000$ km of the Central and North Atlantic, and Northwest and Southeast Indian ridges (CATL, NATL, NWIR and SEIR, respectively; Fig. 2a). These marked differences in MOR migration patterns remain even when spreading rate variations are taken into account (Fig. 2b).

We observe evidence for elevated upper-mantle temperatures beneath slowly migrating ridges through global correlations between VEM and both P- and S-wave velocity perturbations²⁴ at the depth intervals 100–175 km (Figs 1 and 2f). This observation is consistent with recent observations of increased upper-mantle temperatures (up to 250°C based on MORB geochemistry and seismic tomography) beneath spreading ridge segments located near to deeply sourced plumes¹³.

Comparison of MOR basalt geochemistry²⁵ with VEM for MOR segments distal ($>1,000$ – $1,400$ km; refs 16,26) to ridge–plume interactions (Supplementary Fig. 10) reveals patterns supporting elevated upper-mantle temperatures at segments that are at present sampling high-VEM regions of upper mantle (Fig. 2c–e and Supplementary Fig. 11)—that is, regions that have experienced slow ridge migration and significant melt extraction. We observe a negative trend that exists between VEM and the relatively incompatible $\text{NaO}_{8.0}$ (Fig. 2d), whereas positive trends are observed with both $\text{CaO}/\text{Al}_2\text{O}_3$ and $\text{Fe}_{8.0}$ (Fig. 2c,e), which are known to increase with potential temperature and/or degree of partial melting²⁵. Extraction values below $10 \text{ km}^3 \text{ km}^{-1}$ exhibit a diverse range of major element abundances, representing the traverse of more rapidly migrating MORs over a wide variety of upper-mantle temperatures and compositions.

Distances of 1,000–1,400 km (refs 16,26) are commonly thought to be the limit for plume–ridge interaction. The relationship between VEM and MOR basalt geochemistry at these distal MOR segments ($>1,000$ – $1,400$ km) indicates that slowly migrating ridges are able to ‘draw in’ hotter material, from the plume at the distal ridge–plume interaction, and/or from deeper within the upper mantle. It is likely that both mechanisms operate at most ridge segments and may lead to some of the variation observed in MOR basalt geochemistry.

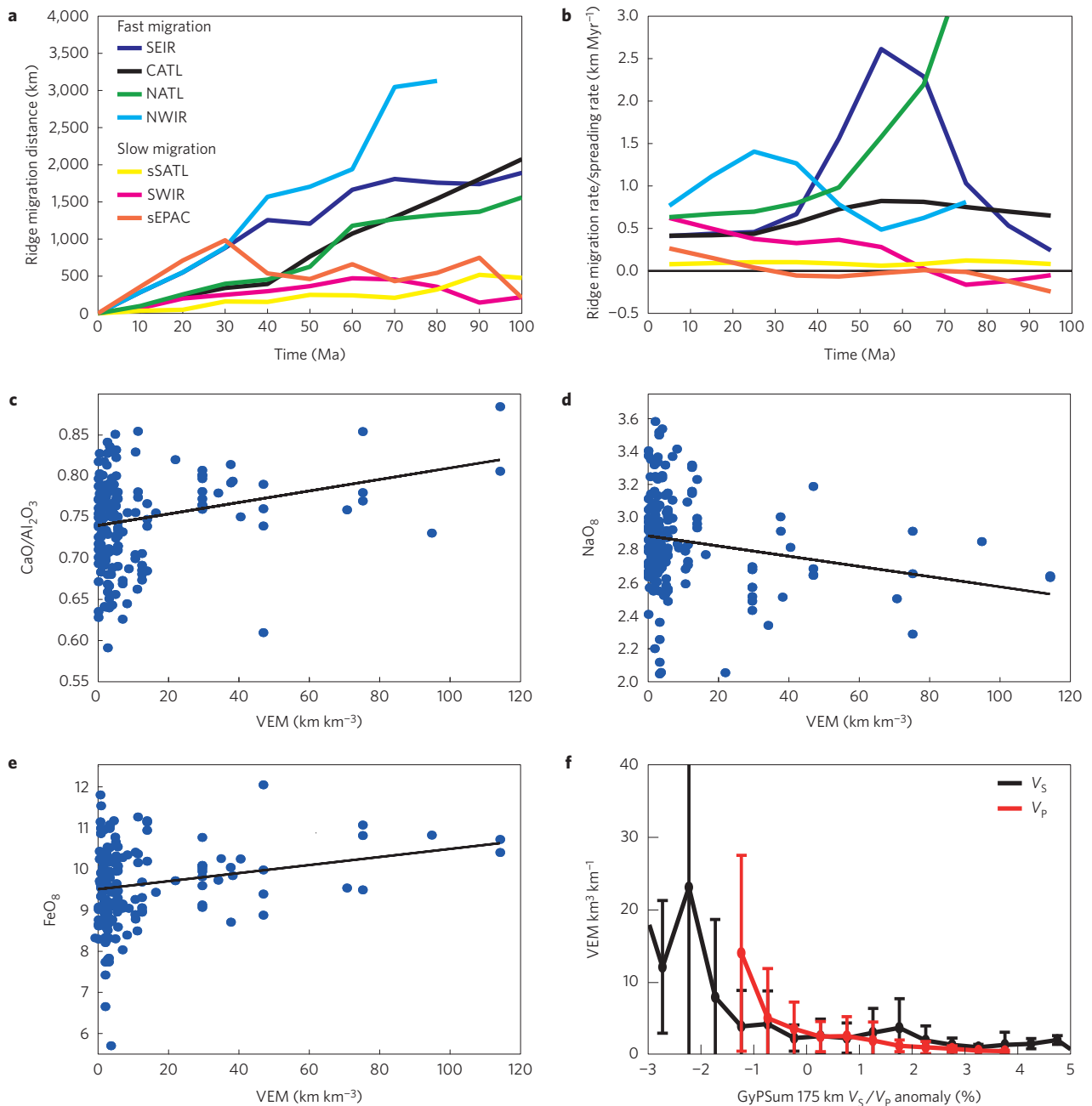


Figure 2 | Regional spatio-temporal MOR migration patterns and comparison of VEM with MOR basalt geochemistry and seismic velocity. **a**, Total ridge migration distance for 0–100 Ma. **b**, Ridge migration rate/spreading rate. **c–e**, Estimated global volume of extracted mantle (VEM) compared with major element geochemistry²⁵, CaO/Al₂O₃ (**c**), Na₂O (**d**) and Fe_{8,0} (**e**), from MOR segments >1,000 km from the nearest deeply sourced plume¹⁹. Black lines—least-squares regression. **f**, Estimated global volume of extracted mantle (VEM) compared with S-wave (black) and P-wave (red) velocity anomalies (100–175 km; ref. 24).

Together, patterns of MOR migration, LIP formation, and correlations of VEM with seismic tomography and MOR basalt geochemistry suggest a strong feedback between the dynamics of slowly migrating ridges and deeply sourced plumes, generated at the edges of LLSVPs, at a global scale, which produce a self-sustained system over timescales up to 180 Myr. The direct interaction of deep plumes with a MOR system tends to anchor the MOR, as indicated by the observed slow migration of MORs (EPAC, SWIR, sSATL) proximal to ridge–plume interactions, probably via a ridge jump mechanism¹². These ridges are characterized by slow migration rates and extract high volumes of melt over extended periods of time, with a continuous draw from the same region of upper mantle.

In our proposed model, MOR segments proximal to the plume are directly affected by the plume, which supplies material to the MOR and affects the temperature beneath the MOR and the MOR basalt composition. The majority of observed LIPs are formed in this region. Plume material will preferentially flow laterally towards areas of elevated lithosphere–asthenosphere interfaces (that is, beneath MORs), with the effect of stabilizing the MOR segment, which stays proximal to the plume via ridge jumps.

Further from the ridge–plume interaction, there is less direct supply of material from the plume to the MOR, but the MOR is affected indirectly via the influence on its migration rate, which is

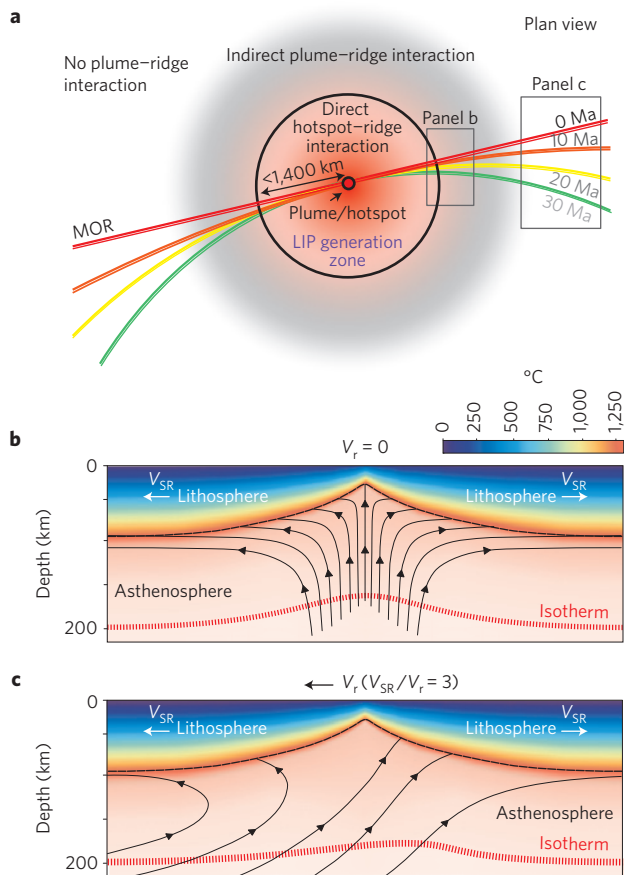


Figure 3 | Schematic representation of the deep plume and shallow mantle upwelling processes at mid-ocean ridges. a, Schematic of interactions between a deeply sourced plume and a MOR. Black circle with red interior represents the plume conduit. Red lines represent the MOR. Coloured lines represent the migration of the MOR in 10 Myr intervals. Boxes outline regions where the processes shown in **b** and **c** would be occurring. **b**, Modelled upper-mantle temperature structure for a stationary MOR, where the ridge velocity is zero. **c**, Modelled upper-mantle temperature structure for a migrating MOR. V_{SR} —spreading rate, V_r —ridge velocity. In **b,c** black lines with arrows show mantle flow and thin dashed red lines show the isotherm.

affected by the distal ‘pinning’ of the MOR to the plume (Fig. 3a). Here, a perturbation of the isotherm directly beneath the MOR occurs (Fig. 3b and Supplementary Fig. 12), as hotter mantle is continually drawn towards the surface by the slowly migrating ridge over long geologic periods (Fig. 3b). This model is supported by observed correlations between VEM and MOR basalt geochemistry at distances $>1,000$ km and seismic tomography (Fig. 2c–f).

Ridge segments located more distally from the ridge–plume interaction are not affected either directly or indirectly by the ridge–plume interaction (Fig. 3a and Supplementary Fig. 12), and are able to migrate more rapidly (Fig. 2a,b). It is possible that these rapidly migrating MORs do not perturb the upper mantle structure significantly, nor focus large volumes of upper mantle towards the MOR (Fig. 3c).

The plumes we have identified as participating in long-standing ridge–plume interactions are possibly sourced from large low shear velocity provinces²². If it is indeed the case that these provinces are stable for very long periods of geologic time (up to 540 Myr; ref. 27), then it is possible that the relationships we observe between plume–ridge interactions and slow MOR migration, as well as their effect on the thermal structure of the upper mantle, are similarly stable. MOR

stability over extended time periods >180 Myr facilitated by ridge–plume interactions has significant implications for the way we model the plate–mantle system, and for understanding observed patterns of ridge morphology and geochemistry.

Methods

Methods and any associated references are available in the online version of the paper.

Received 26 August 2014; accepted 13 April 2015; published online 25 May 2015

References

- Davies, G. F. Plates and plumes: Dynamics of the Earth’s mantle. *Science* **257**, 493–494 (1992).
- Coffin, M. F. & Eldholm, O. Large igneous provinces—crustal structure, dimensions, and external consequences. *Rev. Geophys.* **32**, 1–36 (1994).
- Seton, M. *et al.* Global continental and ocean basin reconstructions since 200 Ma. *Earth-Sci. Rev.* **113**, 212–270 (2012).
- Dickson, G. O., Pitman, W. C. & Heintzler, J. R. Magnetic anomalies in the South Atlantic and ocean floor spreading. *J. Geophys. Res.* **73**, 2087–2100 (1968).
- Zhong, S. J. & Gurnis, M. Mantle convection with plates and mobile, faulted plate margins. *Science* **267**, 838–843 (1995).
- Stein, S., Melosh, H. J. & Minster, J. B. Ridge migration and asymmetric sea-floor spreading. *Earth Planet. Sci. Lett.* **36**, 51–62 (1977).
- Davis, E. E. & Karsten, J. L. On the cause of the asymmetric distribution of seamounts about the Juan De Fuca ridge—ridge-crest migration over a heterogeneous asthenosphere. *Earth Planet. Sci. Lett.* **79**, 385–396 (1986).
- Carbotte, S. M., Small, C. & Donnelly, K. The influence of ridge migration on the magmatic segmentation of mid-ocean ridges. *Nature* **429**, 743–746 (2004).
- Scheirer, D. S., Forsyth, D. W., Cormier, M. H. & Macdonald, K. C. Shipboard geophysical indications of asymmetry and melt production beneath the East Pacific Rise near the MELT experiment. *Science* **280**, 1221–1224 (1998).
- Small, C. & Danyushevsky, L. V. Plate-kinematic explanation for mid-ocean-ridge depth discontinuities. *Geology* **31**, 399–402 (2003).
- Wilson, J. T. Evidence from ocean islands suggesting movement in the Earth. *Phil. Trans. R. Soc. Lond. A* **258**, 145–165 (1965).
- Müller, R. D., Roest, W. R. & Royer, J.-Y. Asymmetric seafloor spreading expresses ridge–plume interactions. *Nature* **396**, 455–459 (1998).
- Dalton, C. A., Langmuir, C. H. & Gale, A. Geophysical and geochemical evidence for deep temperature variations beneath mid-ocean ridges. *Science* **344**, 80–83 (2014).
- Husson, L. & Conrad, C. P. On the location of hotspots in the framework of mantle convection. *Geophys. Res. Lett.* **39**, L17304 (2012).
- Jellinek, A. M., Gonnermann, H. M. & Richards, M. A. Plume capture by divergent plate motions: Implications for the distribution of hotspots, geochemistry of mid-ocean ridge basalts, and estimates of the heat flux at the core–mantle boundary. *Earth Planet. Sci. Lett.* **205**, 361–378 (2003).
- Ribe, N. M. The dynamics of plume–ridge interaction. 2. Off-ridge plumes. *J. Geophys. Res.* **101**, 16195–16204 (1996).
- Richards, M. A., Duncan, R. A. & Courtillot, V. E. Flood basalts and hot-spot tracks: Plume heads and tails. *Science* **246**, 103–107 (1989).
- Garnero, E. J., Lay, T. & McNamara, A. Implications of lower-mantle structural heterogeneity for the existence and nature of whole-mantle plumes. *Geol. Soc. Am. Spec. Pap.* **430**, 79–101 (2007).
- Courtillot, V., Davaille, A., Besse, J. & Stock, J. Three distinct types of hotspots in the Earth’s mantle. *Earth Planet. Sci. Lett.* **205**, 295–308 (2003).
- Montelli, R. *et al.* Finite-frequency tomography reveals a variety of plumes in the mantle. *Science* **303**, 338–343 (2004).
- Coffin, M. F. *et al.* Kerguelen hotspot magma output since 130 Ma. *J. Petrol.* **43**, 1121–1139 (2002).
- Torsvik, T. H., Burke, K., Steinberger, B., Webb, S. J. & Ashwal, L. D. Diamonds sampled by plumes from the core–mantle boundary. *Nature* **466**, 352–355 (2010).
- Müller, R. D., Sdrolias, M., Gaina, C. & Roest, W. R. Age, spreading rates and spreading asymmetry of the world’s ocean crust. *Geochem. Geophys. Geosyst.* **9**, Q04006 (2008).
- Simmons, N. A., Forte, A. M., Boschi, L. & Grand, S. P. GpSuM: A joint tomographic model of mantle density and seismic wave speeds. *J. Geophys. Res.* **115**, B12310 (2010).
- Gale, A., Dalton, C. A., Langmuir, C. H., Su, Y. J. & Schilling, J. G. The mean composition of ocean ridge basalts. *Geochem. Geophys. Geosyst.* **14**, 489–518 (2013).

26. Schilling, J.-G. Fluxes and excess temperatures of mantle plumes inferred from their interaction with migrating mid-ocean ridges. *Nature* **352**, 397–403 (1991).
27. Torsvik, T. H. *et al.* Deep mantle structure as a reference frame for movements in and on the Earth. *Proc. Natl Acad. Sci. USA* **111**, 8735–8740 (2014).
28. Becker, T. W. & Boschi, L. A comparison of tomographic and geodynamic mantle models. *Geochem. Geophys. Geosyst.* **3**, 1003 (2002).

Acknowledgements

The figures in this paper were created using GPlates, GMT, ArcGIS and Matlab. J.M.W. was supported by ARC grant DE140100376. S.E.W. and R.D.M. were supported by ARC grant FL0992245. The work of J.C.A. was supported by ARC grant DP120102372. This is contribution 608 from the ARC CoE CCFS (<http://www.ccfs.mq.edu.au>). M.S. was supported by ARC grant DP0987713. J.M.W. and M.S. acknowledge the support of Statoil. P.W. was supported by a University of Sydney International Visiting Research Fellowship.

Author contributions

J.M.W., M.S., R.D.M. and P.W. conceived the hypothesis. S.M., J.C.A., J.M.W. and S.E.W. carried out computations and workflow development. The bulk of the text was written by J.M.W. All authors participated in planning, discussion throughout the project, and editing of the manuscript and figures.

Additional information

Supplementary information is available in the [online version of the paper](#). Reprints and permissions information is available online at www.nature.com/reprints. Correspondence and requests for materials should be addressed to J.M.W.

Competing financial interests

The authors declare no competing financial interests.

Methods

We quantify palaeo-relationships between LIPs (ref. 2), MORs and plumes (Fig. 1) using a recent global plate tectonic reconstruction³, including reconstructed absolute positions of ridges, continental rifts and LIPs, and a Pacific hotspot reference frame²⁹ which we fix at 145 Myr. For times older than 145 Myr in the Pacific we freeze the reference frame at 145 Myr. For each LIP at its time of formation, we compute using GPlates both the distance to the closest deeply sourced plume^{19,20} and the distance to the closest plate boundary, including regions of diffuse deformation. A key assumption in this analysis is that all plumes have been active since 140 Myr ago, the age of the oldest major oceanic LIP assessed. We acknowledge that it is unlikely that all plumes have been active over this entire period. This assumption, however, errs on the side of caution and allows us to test for previously unknown associations.

To test the influence of alternative reference frames on the proximity among plumes, LIPs and MORs, we tested a number of absolute reference frames in the Indo-Atlantic and Pacific domains (see Supplementary Table 3). There is a small amount of variation in the overall distance between LIPs and the closest plume at formation, but at insufficient levels to change our results in any meaningful way.

We are interested in comparing the MOR migration patterns for different ocean basins, so we compute ridge migration distances and rates for selected regions (Fig. 2). We calculate the average distance from a specified point on the present-day mid-ocean ridges to the point of intersection between the reconstructed MORs and cross-sections oriented in the direction of spreading spaced at 500 km. To account for any influence of spreading rates on migration rates we compute the ratio of migration rate/spreading rate for each system (Fig. 2a,b).

To quantify ridge migration rates, taking into account spreading rates globally, we create and use a global map of the relative volumes of upper-mantle material that have been extracted through partial melting at MORs, per kilometre of overlying ridge length, over the past 140 Myr (Fig. 1 and Supplementary Fig. 5 for workflow).

The map is based on the seafloor spreading and ridge migration histories of the global MOR system²³ (Fig. 1 and Supplementary Figs 7 and 8) and is used as a proxy for the extent of melt extraction of the uppermost mantle. Relative upper-mantle extraction is therefore estimated from the age distributions of the reconstructed MOR spreading segments (Fig. 1a) and their full spreading rates. Relative mantle extraction is expressed in terms of volume per kilometre of ridge length ($\text{km}^3 \text{km}^{-1}$; Supplementary Fig. 9). Regions exhibiting large upper-mantle extraction values correspond to extensive partial melting for long periods of time, whereas regions that have not experienced ridge activity in the past 140 Myr have been masked out of the final map.

Our map of relative upper-mantle volume of extracted mantle is estimated by reconstructing the absolute palaeo-positions of spreading segments of mid-ocean ridges (MORs) at 1 Myr intervals for the past 140 Myr, using a recent seafloor isochrons and plate reconstruction model²³. Transform segments are excluded from the analysis because they do not contribute directly to the extraction of material from the asthenosphere. Reconstruction of palaeo-MORs yields 17,130 irregularly spaced points corresponding to palaeo-MOR positions and their associated reconstruction ages and full seafloor spreading rates. Stage rotations are obtained from the plate reconstruction model, for consecutive age points that are separated by 1 Myr intervals. Full seafloor spreading rates are then calculated from the small circle distance that each of these age points has traversed within each 1 Myr interval.

Supplementary Fig. 5 is a schematic of how the units of relative VEM have been determined. The interquartile age range (Myr) multiplied by full seafloor spreading rate (km Myr^{-1}) represents the width of crust (in km) that has been generated by seafloor spreading, perpendicular to the mean MOR axis within each grid cell. This width is multiplied by a thickness of 7 km, representing the average thickness of oceanic crust that has been removed from the upper mantle to form new crust at MORs over the past 140 Myr. In reality, dynamic processes within the asthenosphere that are associated with seafloor spreading are likely to occur up to significantly greater depths. The objective here, however, is to map the relative extent of upper-mantle extraction: for simplicity, we assume that the thickness of asthenospheric material that has been extracted to form new crust is geographically constant; this thickness is essentially irrelevant for the purposes of assessing relative volumes of extraction. The cross-sectional area of the amount of material that has been extracted over the past 140 Myr represents the volume per kilometre of the average ridge length ($\text{km}^3 \text{km}^{-1}$) within each grid cell. To express mantle extraction as a volume of material beneath each grid cell (that has been subject to extraction through partial melting), one would need to multiply each grid cell value by a known mean ridge length; these lengths are not static over time and are inherently difficult to quantify. Again, for the purposes of mapping relative mantle extraction (VEM), units of volume per kilometre of ridge length are sufficient.

The volume of upper-mantle material extracted from a region during a finite time interval is a function of both the length of time that partial melting has

occurred beneath a MOR (that is, the residence time of migrating ridges above absolute regions of upper mantle) and the rate at which material is extracted. The absolute regions of upper mantle for which VEM is estimated are defined by dividing the Earth's surface into equal-area grid cells. To determine a suitable resolution for the area of these regions, we divide the Earth's surface into grid cells of different resolutions. The number of irregularly spaced reconstructed palaeo-MOR points that lie within each grid cell is then evaluated for each grid resolution. We select a $5^\circ \times 5^\circ$ grid as a good trade-off between the majority of grid cells containing over 15 irregularly spaced palaeo-MOR points (to evaluate the overlying ridge residence time) and the desired high resolution for the final relative VEM map. A large number of reconstructed age points per cell improves the quality of ridge-age distribution analysis in the construction of the final map. The selected grid is relatively coarse, but is suitable for the purpose of identifying and correlating predicted relative VEM with large-scale upper-mantle features. Some grid cells inevitably lack any reconstructed ridge data, and are ultimately masked out of the final map.

We test the age distributions of irregularly spaced points that lie within individual cells of our global $5^\circ \times 5^\circ$ grid to determine a suitable age parameter for the approximation of ridge residence times, including total age range, interquartile age range (that is, the set of ages that excludes the upper and lower quartiles) and standard deviation (Supplementary Fig. 6). We compute each of these age parameters for each grid cell, and calculate the differences between these parameters to identify grid cells where they differ significantly from each other. Twenty four grid cells have been identified from regions with comparatively large differences between the three age parameters, and their age distributions are examined.

Based on our age analysis (Supplementary Fig. 7) we have selected interquartile age range as a proxy for ridge residence time within each grid cell. Unlike total age range, interquartile age ranges are more robust and less likely to contain anomalous age points, whilst still exhibiting larger ranges in regions that have been sampled by ridges for long durations. High interquartile age ranges indicate that a slowly migrating spreading centre has extracted asthenospheric material over a longer period. Mean full palaeo-seafloor spreading rate is used to approximate the rate of extraction of asthenospheric material occurring within each grid cell over the past 140 Myr (Supplementary Fig. 7).

We generate $5^\circ \times 5^\circ$ grids of both full spreading rate and interquartile age (Supplementary Fig. 8), which represent the rate at which material is extracted from the upper mantle and the duration of extraction, respectively. Our final predicted relative upper-mantle VEM grid is constructed by multiplying interquartile age range, full seafloor spreading rate and a thickness of 7 km. The latter represents the average thickness of oceanic crust that has been removed from the upper mantle to form new crust at MORs over the past 140 Myr.

Our quantitative comparison between predicted VEM and seismic velocity perturbations follows a previous methodology where each cell within the grids that are to be compared is assigned to a bin according to its value. The following grids and bin sizes are used: VEM ($5,000 \text{ km}^3 \text{ km}^{-1}$), P- and S-wave velocity anomaly (0.1%). The median VEM value and standard deviation from the median is then calculated for each bin (Supplementary Fig. 3). Grid cell values are also weighted by $\cos \lambda$, where λ is latitude; this accounts for the latitudinal variation in grid cell area.

We compare MOR basalt geochemistry²⁵ with VEM for MOR segments distal ($> 1,000 \text{ km}$) to ridge-plume interactions, focusing on $\text{CaO}/\text{Al}_2\text{O}_3$, $\text{Na}_{8,0}$ and $\text{Fe}_{8,0}$. We calculate a line of best fit using an iteratively reweighted least-squares regression with a bisquare weighting function.

Figure 3b,c are based on numerical experiments solving the 2D equations of conservation of energy, momentum and mass for an incompressible, viscous (Newtonian) fluid³⁰ (Supplementary Methods). Small-scale convection was suppressed (by using a relatively high activation energy) to highlight the first-order flow pattern. The ridge migration velocity is implemented as a velocity boundary condition at the bottom of the model (as the reference frame is fixed at the migrating ridge). Lateral boundary conditions are external no-slip³⁰.

VEM grid, rotation files and ASCII and shapefiles of paleo-MORs, hotspots, and LIPs are available from <http://www.earthbyte.org/resources.html>.

Code availability. Gplates plate tectonics software is available at <http://www.gplates.org>. The code used to compute the volume of extracted mantle (VEM) is not available.

References

- Wessel, P. & Kroenke, L. W. Pacific absolute plate motion since 145 Ma: An assessment of the fixed hot spot hypothesis. *J. Geophys. Res.* **113**, B06101 (2008).
- Gerya, T. *Introduction to Numerical Geodynamic Modelling* (Cambridge Univ. Press, 2009).